El Niño Southern Oscillation evolution modulated by Atlantic forcing

Y. Chikamoto[1*], Z. F. Johnson[1], S.-Y. Simon Wang[1], M. J. McPhaden[2] and T. Mochizuki[3,4]

[1]Department of Plants, Soils & Climate, Utah State University, Logan, UT, USA
[2]Pacific Marine Environmental Laboratory/NOAA, Seattle, WA, USA
[3]Department of Earth and Planetary Sciences, Kyushu University, Fukuoka, Japan
[4]Japan Agency for Marine-Earth Science and Technology, Yokohama, Japan

Key Points:

- Model runs show that equatorial Atlantic warming (cooling) triggers subsequent tropical Pacific cooling (warming) 7 months later.
- Pacific wind-SST feedbacks are robust on ENSO timescales, but model sensitivity is large in Pacific wind response to Atlantic forcing.
- El Niño Southern Oscillation predictability is modulated by the Atlantic mean state bias and systematic errors in inter-basin interactions.

*4820 Old Main Hill, Logan, UT 84322-4820, USA

Corresponding author: Yoshimitsu Chikamoto, `yoshi.chikamoto@usu.edu`

Abstract

The El Niño Southern Oscillation (ENSO) exerts a strong influence on tropical Atlantic variability, but it is also affected by Atlantic forcing. Previous research has proposed three Atlantic precursors for ENSO: the North tropical Atlantic, the equatorial Atlantic, and the entire tropical Atlantic. However, the relative importance of these Atlantic precursors for ENSO remains unclear. Here, we present evidence from a set of multi-model partial ocean assimilation experiments that equatorial Atlantic cooling is the main contributor for weakening equatorial zonal winds in the Indo-Pacific sector and subsequent ocean warming in the tropical Pacific. Opposite tendencies occur for a warmer equatorial Atlantic. The equatorial Atlantic affects the inter-basin climate seesaw between the Atlantic and Pacific through an atmospheric zonal wavenumber 1 pattern. However, model mean-state biases and systematic errors prevent a precise assessment of the response times for the equatorial Pacific trade winds to Atlantic forcing.

Plain Language Summary

El Niño—an unusual surface warming of the tropical Pacific—may be more predictable than previously thought if the prediction of Atlantic climate and its remote impact on the Indo-Pacific region can be improved. In this study, we found that sea surface cooling in the equatorial Atlantic weakens western Pacific trade winds and triggers subsequent tropical Pacific warming through a positive feedback of atmosphere-ocean interactions. This process increases the chance of an El Niño event 7 months later. By assimilating observed ocean data in this simulation, we found that El Niño predictive skill relies not only on the tropical Pacific climate state but also on the Atlantic mean state and its remote impact on the tropical Pacific. Our result suggests that improving model performance in the Atlantic ocean and its remote impacts are crucial for enhancing El Niño predictions.

1 Introduction

Tropical Pacific climate variability has profound impacts not only on the Pacific region but also on global climate, including the Atlantic Ocean. A well-known example is the remote influence of the El Niño Southern Oscillation (ENSO) on Atlantic sea surface temperature (SST) variability, particularly in tropics north of the equator (Timmermann et al., 2018; S. P. Xie & Carton, 2004). The opposite pathway also exists, that is, the

Atlantic can affect tropical Pacific climate variability (e.g., Cai et al., 2019, and references therein). Consistent with this pathway, the tropical Pacific SST predictability is enhanced when precursor signals in the tropical Atlantic Ocean are taken into account in statistical ENSO prediction models (Frauen & Dommenget, 2012; Dayan et al., 2014; Martín-Rey et al., 2015) as well as in a dynamical model (Keenlyside et al., 2013). However, the two-way interaction between the tropical Pacific and the Atlantic makes it challenging to identify the dynamics and mechanisms involved in the Atlantic precursor of ENSO predictability. According to ENSO recharge theory (Jin, 1997), the evolution, termination, and flavors of ENSO events are attributed to upper ocean heat content and trade wind anomalies in the tropical Pacific (Timmermann et al., 2018; Meinen & McPhaden, 2000). Whereas heat content variability is controlled by ocean dynamics within the tropical Pacific (C. Wang & Picaut, 2004), trade wind variability can be modulated by local stochastic processes (Timmermann et al., 2018) as well as the remote forcing from the Atlantic (Cai et al., 2019, and references below), the Indian Ocean (S. Xie et al., 2009; Izumo et al., 2010, 2014; Dong & McPhaden, 2018), and the subtropical western North Pacific (S.-Y. Wang et al., 2013; Fosu et al., 2020).

To better understand precursors to the remote forcing of ENSO, this study focuses on the Atlantic impact on the trade wind variability and subsequent ENSO evolution. Three precursors of SST variability have been proposed for the tropical Atlantic impact on ENSO: the equatorial cold-tongue (i.e., the Atlantic Niño; Rodríguez-Fonseca et al., 2009; Ding et al., 2012; Keenlyside et al., 2013; Martín-Rey et al., 2014; Polo et al., 2015), the North tropical Atlantic (Ham, Kug, Park, & Jin, 2013; Ham, Kug, & Park, 2013; L. Wang et al., 2017), and the entire tropical Atlantic (Kucharski et al., 2011, 2016; McGregor et al., 2014; Chikamoto et al., 2015; Li et al., 2015; Ruprich-Robert et al., 2017). On seasonal-to-interannual timescales, the most prominent precursor is the Atlantic cold-tongue, in which an Atlantic Niño during the boreal summer can trigger a Pacific La Niña event in the subsequent winter through modulation of the global Walker circulation (Rodríguez-Fonseca et al., 2009; Keenlyside et al., 2013). This relationship is also found in the opposite phase (i.e., the Atlantic Niña and the Pacific El Niño). Another precursor is also proposed on seasonal-to-interannaul timescales: SST anomalies in the Northern tropical Atlantic during the boreal spring can affect ENSO events in the following winter through changes in the North Pacific subtropical high (Ham, Kug, Park, & Jin, 2013; Ham, Kug, & Park, 2013; L. Wang et al., 2017). On decadal-to-multidecadal timescales, by contrast, SST warming in the entire tropical Atlantic could be an important driver for a La Niña-like climate response in the tropical Pacific, which corresponds to more frequent and prolonged La Niña events for all seasons through the reorganization of the global Walker circulation and subsequent atmosphere-ocean interactions (Kucharski et al., 2011, 2016; McGregor et al., 2014; Chikamoto et al., 2015; Li et al., 2015; Ruprich-Robert et al., 2017). These studies prompt the question about which part of the tropical Atlantic is more important for inter-basin climate interactions on decadal timescales: the North tropical Atlantic associated with the Atlantic Multidecadal Oscillation (Kucharski et al., 2016; Levine et al., 2017; Ruprich-Robert et al., 2017), the equatorial Atlantic (McGregor et al., 2014), or the South tropical Atlantic (Chikamoto et al., 2016; Barichivich et al., 2018). Such differences in perspective may result from seasonal dependencies and model sensitivities in the Atlantic impacts on ENSO. Even without seasonal dependence, a question still remains as to which part of the Atlantic Ocean is most important for modulating the interannual ENSO evolution.

To evaluate Atlantic impacts on the tropical Pacific climate variability, several model experiments have been proposed. One of the common approaches is the Atmospheric Model Intercomparison Project (AMIP)-type experiment, in which an atmospheric general circulation model is forced by observed SST variability using a slab ocean model (e.g., McGregor et al., 2014). AMIP-type experiments can evaluate the direct atmospheric response to Atlantic SST forcing, but they do not capture the time evolution of dynamical atmosphere-ocean responses due to the lack of an ocean dynamical model. To retain dynamical atmosphere-ocean interactions in response to ocean remote forcing, some studies conducted the Atlantic forcing experiments using an intermediate complexly atmospheric model (so-called SPEEDY) coupled with a 1.5 layer reduced gravity ocean model (Rodríguez-Fonseca et al., 2009) or ocean general circulation model (Kucharski et al., 2016). However, those experiments required flux adjustment to avoid artificial "model drift" during the simulations, which can obscure the identification of crucial mechanisms. This issue motivates advanced model experiments using a fully coupled dynamical model, such as pacemaker experiments by nudging the model to the observed SST (Ding et al., 2012; Keenlyside et al., 2013; Kosaka & Xie, 2013; Li et al., 2015) or partial assimilation experiments as described below.

To identify the most prominent Atlantic precursor for modulating the interannual ENSO evolution without seasonal dependence (i.e., focusing on a 12-month mean instead of a seasonal mean), this study applies a partial ocean assimilation approach based on three sets of experiments. In these partial assimilation experiments, observed 3-dimensional ocean temperature and salinity fields for the targeted region are assimilated into the ocean component of the global climate models. By assimilating the observed fields only in the Atlantic Ocean as described in Section 2, we can estimate the Atlantic contribution to tropical Pacific climate variability. Using these experiments, Section 3 illustrates the process by which Atlantic Ocean variability affects the evolution of ENSO as well as the sensitivity in those processes. Results are discussed in Section 4 and summarized in Section 5.

2 Model setup and Data

2.1 Model experiments

Main configurations of the partial ocean assimilation experiments are based upon the decadal climate prediction systems developed from two global climate models: MIROC3.2 (Nozawa et al., 2007) and CESM1.0 (Shields et al., 2012). Both models consist of fully coupled general circulation models of atmosphere, land, ocean, and sea-ice components. MIROC3.2 has a T42 spectral grid for atmosphere and land components whereas ocean and sea-ice components consist of a latitude-longitude coordinate with an approximately 0.56-1.4° horizontal grid. The CESM1.0 has lower resolution than the MIROC3.2: a T31 spectral grid for atmosphere and land components and a curvature grid with a displaced North Pole for ocean and sea-ice components (approximately 1° latitude and 3° longitude grid near the equator). Those decadal climate prediction systems consist of three basic model experiments (Table 1a): 20^{th} century historical simulations, global ocean assimilation runs, and hindcast runs. In the 20^{th} century historical simulations, we prescribed the natural and anthropogenic radiative forcings (e.g., greenhouse gas and aerosol concentrations, solar cycle variations and major volcanic eruptions) for 1850–2005. After 2005, we prescribed the A1B-type emission scenario for MIROC and the RCP4.5 scenario for CESM. These experiments consist of 10 ensemble members conducted with initial conditions obtained from 10 random years of the pre-industrial control simulations. In the global ocean assimilation runs, we use the same model configuration with the historical simulations but assimilate the observed 3-dimensional ocean temperature and salinity anomalies into the ocean component of global climate models. In the assimilation process, the monthly observations were linearly interpolated to daily fields. Analysis increments are estimated from a temporally, spatially, and vertically invariant model-to-observation ratio in analysis errors and added as forcing into the model's temperature and salinity tendency equations during an analysis interval of one day (Mochizuki et al., 2010; Tatebe et al., 2012) using an Incremental Analysis Update scheme (Bloom et al., 1996; Huang et al., 2002). Observations were derived from the objective analysis compiled by the Japan Meteorological Agency (referred to as ProjD; Ishii & Kimoto, 2009) for 1945–2010 in MIROC, and from the ECMWF ocean reanalysis product version 4 (Balmaseda et al., 2013) for 1958–2014 in CESM. The initial 5 and 2 years of model integrations were excluded in MIROC and CESM, respectively, as the model spin-up period. Climatological fields are calculated based on each observation and model historical simulations for a reference period of 1971–2000. Whereas 3-dimensional oceanic anomalies are derived from the climatological fields in MIROC (Mochizuki et al., 2010), the model biases of historical simulations are further adjusted in CESM (Chikamoto et al., 2019). More detailed descriptions and the performance of these decadal climate prediction systems are found in previous studies for the MIROC (Mochizuki et al., 2010; Chikamoto et al., 2012; Mochizuki et al., 2012; Tatebe et al., 2012; Chikamoto et al., 2013) and the CESM (Chikamoto et al., 2017, 2019).

Using the same configurations of global ocean assimilation runs in MIROC3.2 and CESM1.0, we conducted three sets of Atlantic Ocean partial assimilation runs. The three experiments are summarized in Table 1b, namely the MIROC ATL anomaly, CESM ATL anomaly, and CESM ATL full runs. In all of these ATL runs, observed 3-dimensional fields of ocean temperature and salinity in the Atlantic Ocean were assimilated into the ocean components of MIROC and CESM, in the same way as the global ocean assimilation runs but targeted on the Atlantic Ocean only (50°S–60°N for MIROC and 30°–70°N for CESM). The main advantage in our partial assimilation approach is that, by assimilating 3-dimensional ocean fields, the models are able to simulate ocean variability in the mixed layer and thermocline more appropriately compared to SST-only assimilation runs and pacemaker experiments (Chikamoto et al., 2019; Ding et al., 2012). Whereas the MIROC and CESM ATL "anomaly" runs assimilate observed "anomalies" with maintaining model climatological fields, the CESM ATL "full" run incorporates full-field observations (i.e., observed anomaly plus observed climatology) instead of the anomaly field only. As a result, the CESM ATL full runs have the smallest biases of climatological ocean fields in the assimilated Atlantic region, whereas MIROC and CESM ATL anomaly runs still exhibit model mean state biases but suppress artificial shock for model states during assimilation (left panels in Fig. 1). It is interesting to note that, even though the climatological SST biases in the Atlantic are almost negligible in the CESM ATL full run, we can still find SST and SLP biases in the tropical Pacific (Fig. 1e and f). The SST and SLP biases show different patterns among three Atlantic partial assimilation experiments (Fig. 1) since our multi-model approach tends to cover a diverse set of Atlantic forcing experiments. Therefore, our model experiments provide a perspective on model sensitivity, involving model systematic errors (MIROC ATL anomaly vs CESM ATL anomaly runs) and climatological mean state biases (CESM ATL anomaly vs full runs).

It is worth noting the difference between "pacemaker experiments" and partial assimilation experiments being conducted here. Both use fully coupled atmosphere-ocean general circulation models without any flux adjustment. In pacemaker experiments, a fully coupled atmosphere-ocean model is forced by the observed SST field for a targeted region but is allowed to evolve freely outside the targeted region. Using the pacemaker experiment targeted for eastern tropical Pacific SST, for example, Kosaka and Xie (2013) demonstrated that the recent global warming hiatus could be mainly attributed to eastern tropical Pacific SST variability. Ding et al. (2012) also illustrated the Atlantic Niño impact on the amplitude of ENSO events based on pacemaker experiments by prescribing the observed SST field in the tropical Atlantic. However, a recent study in the Coupled Model Intercomparison Project Phase 6 (CMIP6) Decadal Climate Prediction Project-Component C coordination pointed out that the Atlantic SST forcing in pacemaker experiments may introduce energy and seawater density imbalances due to a lack of salinity information, which causes an artificial change in the air-sea interaction and alters the coupled model equilibrium (Boer et al., 2016). In the equatorial Pacific, SST is the main driver for mixed layer dynamics through strong atmosphere-ocean interaction, which can constrain tropical Pacific climate variability. In the Atlantic and extra-tropics, however, subsurface ocean temperature and salinity also play an important role in ocean dynamics. Hence, SST-only assimilation is not sufficient to constrain the ocean density structure due to higher-frequency fluctuations. As a result, SST-only assimilation or pacemaker approaches may fail to properly simulate the observed SST variability (Chikamoto et al., 2019). To avoid this situation, pacemaker experiments "strongly" nudge models toward the observed SST (a typical restoring timescale is order 1–10 days for a 50 m mixed layer depth). Such observed SST is usually monthly mean values so that strong nudging damps higher-frequency atmosphere-ocean interaction at sub-monthly timescales. Because higher-frequency atmosphere-ocean interactions are important for the model to adjust toward quasi-equilibrium climate states, the strong SST constraint in pacemaker experiments may cause artificial model drift and energy imbalances. In addition to this energy imbalance during the nudging process, most global climate models suffer from a climatological SST bias with a colder northern tropical Atlantic and a warmer southeastern tropical Atlantic (Richter, 2015), which distorts the Atlantic impact on tropical Pacific climate variability (Sasaki et al., 2014; McGregor et al., 2018; Kajtar et al., 2018; Luo et al., 2018). The partial ocean assimilation approach can minimize the artificial influence of model drift and energy imbalances on inter-basin climate interactions. In this approach, the observed SST variability is "weakly" assimilated into the models in order to allow models to adjust the model-simulated quasi-equilibrium condition (a typical restoring timescale is much larger than 10-days). By assimilating subsurface ocean temperature and salinity, the model better simulates lower-frequency ocean dynamics, which can provide more realistic simulation of observed SST variability compared to SST-only assimilation (Chikamoto et al., 2019). As a result, partial assimilation experiments, compared to pacemaker experiments, have the advantage of minimizing artificial model drift in response to prescribed ocean forcing.

2.2 Data sources

We use several gridded observations to minimize observational uncertainty. Observed sea level pressure (SLP) and zonal winds at 250 (U250) and 850 hPa (U850) are obtained from NCEP-NCAR (Kalnay et al., 1996) and JRA55 atmospheric reanalyses (Kobayashi et al., 2015). SST datasets include ERSST version 4 (Huang et al., 2015) and an objective ocean analysis compiled by the Japan Meteorological Agency (i.e., ProjD; Ishii & Kimoto, 2009). Anomalies are defined as deviations from the climatological mean for the 50-year period 1960–2009 in each of the model experiments and observations. All anomalies are detrended using a least-squares quadratic trend and are re-gridded into a $2.5^\circ \times 2.5^\circ$ latitude-longitude grid. A 12-month running mean filter is applied to all anomalies to minimize the effect of seasonality. The multi-model ensembles are obtained by averaging the three Atlantic partial assimilation runs after taking the ensemble mean of 10 members for each model experiment during the 1960–2009 period, whereas observational estimates are based on the average of the two reanalysis products during the same period as the model. To focus on interannual ENSO variability forced by the Atlantic, the Niño 3.4 index is smoothed by applying a 12-month running average to monthly SST anomalies over the Niño 3.4 region (5°S–5°N, 120°W–170°W) in observations and ATL runs individually. Whereas the observed Niño 3.4 index shows a prominent seasonality with a peak during boreal winter, such seasonality for the model simulated Niño 3.4 index is much reduced in the ATL runs even at monthly resolution (Fig. 2a). This result suggests that the Atlantic impact on ENSO can occur in any season even though the Atlantic Niño is prominent during the boreal summer (Fig. 2b).

3 Results: Tropical Pacific climate response to Atlantic forcing

To depict the temporal evolution of ENSO, we first produced the lead-lag correlation maps of SST and SLP anomalies associated with the Niño 3.4 index (5°S–5°N, 120°W–170°W) in the observation-based data and multi-model ensembles of the three ATL runs (Fig. 3). Observational analysis demonstrates the zonal gradients of SST and SLP anomalies between the western and eastern tropical Pacific during the decaying stage of La Niña events at −18 month lag (Fig. 3a) and then an opposite phase of those gradients during the mature stage of El Niño events at 0-month lag (Fig. 3g), confirming previous findings (Timmermann et al., 2018; Meinen & McPhaden, 2000; Jin, 1997). In the tropical Atlantic, unusually cold SST appears around the equator during the developing phase of El Niño at −12 and −6 months lag (Fig. 3c and e) and then decays during the mature phase of El Niño at 0-month lag (Fig. 3g). This lead-lag relationship between ENSO and equatorial Atlantic SST anomalies accompanies the SLP contrast between the Atlantic and the eastern Pacific, reflecting the reorganization of the global Walker circulation as reported previously (Rodríguez-Fonseca et al., 2009; Ham, Kug, Park, & Jin, 2013; Ham, Kug, & Park, 2013; Cai et al., 2019). In the statistical analysis of observations, however, the causality remains unclear as to whether colder SST in the equatorial Atlantic is affecting ENSO evolution (Rodríguez-Fonseca et al., 2009; Ding et al., 2012; Keenlyside et al., 2013; Martín-Rey et al., 2014; Polo et al., 2015) or if it is simply a response to the remote impact of ENSO (Enfield & Mayer, 1997; Latif & Grötzner, 2000; Handoh et al., 2006; Lübbecke & McPhaden, 2012; Tokinaga et al., 2019).

3.1 Processes

Through the Atlantic Ocean assimilation experiments, the Atlantic impact on ENSO can be revealed more clearly (right panels in Fig. 3). ATL runs constrain only Atlantic Ocean variability and the 10-member ensemble mean in each ATL run filters out the internally generated ENSO variability within the Pacific Ocean, so we can assume that any simulated ENSO variability in the ATL run originates from the Atlantic Ocean forcing. In other words, the ATL run emphasizes the one-way impact from the Atlantic to the Pacific since the observations assimilated into the ATL run may include two-way interactions between these basins. At −18 month lag, the multi-model ensemble of ATL runs shows the initiation of colder SST and higher SLP anomalies in the north tropical Atlantic (Fig. 3b). These Atlantic SST and SLP anomalies in the equatorial band reach maturity from −12 to −6 months lag, coinciding with the developing stage of El Niño (Fig. 3d and f). While the Atlantic SST anomaly develops, a zonal SLP gradient emerges in the equatorial Indo-Pacific region at −12 months lag and then strengthens afterward. This zonal SLP gradient arguably causes anomalous westerly winds in the Indo-Pacific region (i.e., weakened Pacific trade winds). This process is known to trigger equatorial Pacific SST warming through the Bjerknes feedback, leading to the mature stage of El Niño (Rodríguez-Fonseca et al., 2009; Polo et al., 2015). Once the Bjerknes feedback is activated, ENSO can develop through internal tropical Pacific dynamics without much input from the Atlantic (Fig. 3h and j). Regression maps associated with the Niño 3.4 index also show consistent results (Fig. S1).

The multi-model ATL run reveals the most prominent precursor for ENSO from equatorial Atlantic SST with −12 to −6 months lag, which supports previous findings about the influence from the boreal summer Atlantic Niño to the following winter ENSO amplitude (Rodríguez-Fonseca et al., 2009; Ding et al., 2012; Keenlyside et al., 2013; Martín-Rey et al., 2014; Polo et al., 2015). In addition, we also find significant negative correlations of SST anomalies in the Northern tropical Atlantic at −18 and −12 months lag, albeit weaker (Ham, Kug, Park, & Jin, 2013; Ham, Kug, & Park, 2013; L. Wang et al., 2017). These Atlantic SST patterns from −18 to −6 months lag are not identical to the temporal evolution of typical Atlantic Niño that has larger SST anomalies in the southeastern tropical Atlantic (S. P. Xie & Carton, 2004; Rodríguez-Fonseca et al., 2009). In any case, we find that equatorial Atlantic SST variability serves as one of the main drivers for ENSO evolution in our experiments.

To facilitate the description of the tropical Pacific response to Atlantic forcing, we produce Hovmöller diagrams (Figs. 4 and 5) for the lead-lag correlations of SST, SLP, U850 and U250 anomalies at the equator with the Niño 3.4 index. In the multi-model ensemble of ATL runs, a local peak of Atlantic SST cooling (60°W–0°) appears around 7 months before the mature stage of El Niño (at −7 months lag in Fig. 4b), which is comparable to the lead-lag relationship between the boreal summer Atlantic Niña and the boreal winter Pacific El Niño (Rodríguez-Fonseca et al., 2009; Ding et al., 2012; Keenlyside et al., 2013; Martín-Rey et al., 2014; Polo et al., 2015). This equatorial Atlantic SST cooling apparently induces positive SLP anomalies over the Atlantic and their subsequent eastward propagation over the Indian Ocean (S.-Y. S. Wang et al., 2015). Concurrently with these SLP responses in the Atlantic and Indian Oceans, we also find a delayed response of negative SLP anomalies in the central and eastern equatorial Pacific. These tropical SLP responses consist of an atmospheric wave-number 1 pattern between the Atlantic-Indian and the Pacific Oceans, resulting in a reorganization of the global Walker circulation in the process. Similar SST and SLP anomalies are found in individual ATL runs, despite a difference in timing of Atlantic SST precursors (Fig. 4c–e). Consistent with the zonal SLP anomaly gradients, anomalous winds in the lower troposphere show westerlies over the Indian and western Pacific Oceans (60°E–150°W) and easterlies over the eastern Pacific and Atlantic Oceans (150°W–0°; shading in Fig. 5d). Similar but opposite patterns are found in the upper tropospheric zonal winds (Fig. 5b). Specifically, anomalous westerly winds at 850 hPa correspond to weakened trade winds in the western equatorial Pacific. The similar changes in the multi-model ATL runs are found in the observations (Fig. 4a), albeit with a delay in the timing of Atlantic SST cooling, an earlier peak of Atlantic SLP anomalies, and a longer duration of SST and SLP anomalies in the tropical Pacific.

3.2 Timing of evolution

To examine the time it takes for ENSO to respond to the Atlantic forcing, we construct additional lead-lag correlations of equatorial Atlantic SST anomalies (5°S–5°N, 50°W–0°) and zonal wind anomalies at 850 hPa in the Indo-Pacific region (averaged in 5°S–5°N, 90°E–150°E) by correlating them with the Niño 3.4 index (Fig. 6). We should note that the multi-model ATL runs exhibit weaker correlations at negative lags (with Niño 3.4 leading) compared to those in observations (black lines in Fig. 6b and c). This weaker correlation of the ATL runs suggests that the multi-model ATL runs emphasize the Atlantic's impact on the response of the zonal winds, whereas this process is obscured in observational analyses because of the two-way inter-basin interaction. The results of the multi-model ATL runs demonstrate that Atlantic SST anomalies negatively correlate with zonal wind anomalies at 850 hPa over the equatorial Indo-Pacific region with a local peak at 0-month lag (red line in Fig. 6a). However, there is a time lag of 7 months in the maximum correlation coefficient between zonal wind anomalies and the Niño 3.4 index (Fig. 6b). In other words, the multi-model ATL runs indicate that the equatorial Atlantic SST cooling induces weakened trade winds in the equatorial western Pacific almost simultaneously as seen in the wave number 1 pattern of SLP anomalies (Fig. 4). Subsequently, the trade wind changes lead to the delayed response of equatorial Pacific SST warming by the activation of the Bjerknes feedback. This argument works for the opposite phases associated with Atlantic SST warming. Consistent with these lead-lag relationships, the correlation of equatorial Atlantic SST anomalies with the Niño 3.4 index shows a local peak at 7 months lag (Fig. 6c). Similar results are also obtained when we apply a 3-month running mean filter (Fig. S2).

For verification purposes, we perform additional composite analysis based on equatorial Atlantic SST anomalies. Using the multi-model ensemble of the ATL runs (Fig. 7), we extract from the equatorial Atlantic the 7 warmest (Aug 1963, Nov 1968, May 1973, Jul 1984, Feb 1988, Mar 1996 and May 1998) and 7 coldest SST anomalies (Feb 1965, Oct 1967, Dec 1971, Aug 1976, Jan 1983, Sep 1992, Apr 1997), regardless of the concurrent ENSO phases. These extracted warmest and coldest years in the ATL runs are identical to the observed warmest and coldest years of the equatorial Atlantic SST anomalies because the ATL runs incorporate the observed information for that region. When we create a histogram of anomalous zonal winds in the Indo-Pacific region based on individual ensemble members, we find a shift in the distribution towards the easterly wind anomalies in the Indo-Pacific region associated with warmer Atlantic SSTs and the westerly anomalies with colder Atlantic SSTs (Fig. 8a). Consistent results are also found in the western Pacific trade winds (Fig. 8b). Since these changes in the trade winds contribute to the evolution of SST anomalies in the equatorial Pacific, one can infer that unusually warm Atlantic SSTs enhance the probability of a La Niña event at +7 months lag (Fig. 8c). This result suggests that equatorial Atlantic SST variability can act as an external forcing for ENSO dynamics by affecting the ENSO probability at least 7 months before the peak phase of the Atlantic forced ENSO event through a modulation of the Pacific trade winds. Of course, ocean dynamics within the tropical Pacific is still the main driver for the development of ENSO even in the presence of external forcing (Jin, 1997; Timmermann et al., 2018).

3.3 Model sensitivity

We note the present model sensitivity regarding the response timescale of ENSO to the Atlantic forcing, recalling that equatorial Atlantic SST anomalies are negatively correlated with the Niño 3.4 index at a lag of +4 months in the CESM ATL anomaly run (blue solid), +5 months in CESM ATL full run (blue dashed), and +12 months in MIROC ATL anomaly run (green line in Fig. 6c), respectively. In contrast to this model sensitivity, the anomalous zonal winds positively correlate with the Niño 3.4 index around +7 months lag in all runs (blue and green lines in Fig. 6b), indicating a minimal discrepancy when it comes to simulating the Bjerknes feedback. However, a larger model sensitivity was found in the local peaks of correlation coefficients between Atlantic SST anomalies and anomalous zonal winds at −1, 0, and +5 months lags in the CESM ATL anomaly (blue solid), CESM ATL full (blue dashed), and MIROC ATL anomaly runs (green line in Fig. 6a), respectively. These time lags show a larger difference between MIROC and CESM runs, compared to the difference between CESM ATL anomaly and full runs. In other words, the Indo-Pacific zonal wind responses to the Atlantic forcing have a larger sensitivity between MIROC and CESM rather than between the CESM anomaly vs full-field assimilations.

In addition to the large sensitivity in the zonal wind response, we also find a large difference in Indian Ocean responses to the Atlantic forcing. Figure 9 shows the Hovmöller diagrams for the lead-lag correlations of U850 and U250 anomalies at the equator with the Niño 3.4 index. Whereas the MIROC ATL anomaly run demonstrates the significant phase changes in U850 anomalies from westerly to easterly over the Indian Ocean (60°E–120°E), the signal is less clear in CESM ATL anomaly and full runs (bottom panels in Fig. 9). Associated with these lower-level wind responses, we can find an opposite sign of upper-tropospheric zonal wind responses aloft in MIROC ATL anomaly run but an obscured response in the CESM ATL anomaly and full runs (top panels in Fig. 9). These upper and lower zonal wind anomalies suggest that the Walker circulation response in Indian Ocean is stronger in the MIROC but weaker in the CESM. Consistent with these wind anomalies, the Indian Ocean SST warming after the mature stage of El Niño is clear in MIROC ATL anomaly run but unclear in CESM ATL anomaly and full runs (bottom panels in Fig. 4). Because of this model sensitivity in the Indian Ocean response, the multi-model ensemble of ATL runs show weaker SST anomalies in the Indian Ocean compared to observations (Figs. 3 and 4a–b).

4 Discussion

Since our Atlantic partial assimilation runs assume "perfect knowledge" of Atlantic Ocean variability, an ENSO anomaly correlation coefficient (ACC) between observation and model simulation corresponds to the potential predictability of ENSO that is driven by Atlantic remote forcing. The potential predictability for Niño 4, Niño 3.4, and Niño 3 indices based on the ATL runs (Table 2) is higher in the MIROC ATL anomaly and CESM ATL full runs (e.g., for Niño 3.4 index, ACC=0.24 and 0.22) than the CESM ATL anomaly run (ACC=0.06). As a result, we can find higher predictability for the anomalous zonal winds in the Indo-Pacific region: ACC=0.23, 0.46, and 0.18 in the MIROC ATL anomaly, CESM ATL full, and CESM ATL anomaly runs, respectively. Consistent with the potential predictability of ENSO, a correlation coefficient between the observed and the model simulated upper ocean heat content in the western equatorial Pacific is higher for the MIROC ATL anomaly (R=0.41) and the CESM ATL full runs (R=0.39) than for the CESM ATL anomaly run (R=0.30; left panels in Fig. S3), though the differences are not statistically significant at the 95% level of confidence. These results suggest that ENSO predictive skill relies not only on tropical Pacific climate states but also on how well models depict the tropical Atlantic SST and Indo-Pacific atmospheric responses to the Atlantic forcing. Further analysis on monthly mean timescales may contribute to advancing our understanding of ENSO predictability, such as the "spring barrier" of ENSO skill reduction (McPhaden, 2003).

Using the statistical and dynamical approaches, previous studies aimed to improve the predictive skills in ENSO amplitude during the mature stage of ENSO events with an emphasis on the seasonal relationship between boreal summer Atlantic Niña and the subsequent winter Pacific El Niño (Frauen & Dommenget, 2012; Keenlyside et al., 2013; Dayan et al., 2014; Martín-Rey et al., 2015). The results of our multi-model approach are also consistent with this seasonally dependent relationship between the equatorial Atlantic and ENSO. By minimizing seasonality in our analysis, we have found that the equatorial Atlantic can influence ENSO predictability not only during its mature stage but also during its onset, decay, and developmental phases. However, there is a large spread for the simulated timing of the Indo-Pacific wind response to the Atlantic forcing. The sensitivity to Atlantic mean state bias therefore introduces an additional source of uncertainty for Atlantic-forced ENSO predictability. Likewise, there is a discrepancy in potential ENSO predictability between our ATL runs and the Atlantic pacemaker experiments conducted by Ding et al. (2012): higher potential predictive skill in the tropical Pacific SST anomalies is found in the west in our ATL run (Table 2 and Fig. S3) but in the east in the pacemaker experiment (Fig 4 in their paper). This discrepancy provides another perspective on the predictability that involves ENSO diversity (Capotondi et al., 2015), which might be modulated by Atlantic mean state biases, model systematic errors, and assimilation methods (Ding, Keenlyside, et al., 2015; Ding, Greatbatch, et al., 2015; Dippe et al., 2019; Johnson et al., 2020). According to previous studies (Ham, Kug, Park, & Jin, 2013; Ham, Kug, & Park, 2013), the boreal summer Atlantic Niño enhances occurrences in the eastern Pacific type of ENSO in the subsequent winter, whereas the spring North Atlantic SST anomalies contribute to an increase in the central Pacific type of ENSO events. To investigate these hypotheses regarding the Atlantic impact on ENSO predictability, more research is necessary to engage in multi-model approaches based on different types of climate models and Atlantic experimental design (e.g., pacemaker and partial assimilation experiments), as well as idealized model experiments prescribing the Atlantic climate modes such as the Atlantic Niño, the meridional mode, and the Atlantic Multi-decadal Oscillation (Ruprich-Robert et al., 2017; Levine et al., 2018).

Previous studies have shown a large inter-model spread regarding the trade wind response to Atlantic forcing on decadal and multi-decadal timescales (McGregor et al., 2018; Kajtar et al., 2018; Luo et al., 2018). Our results show a similar model sensitivity on interannual timescales. Further evaluation is required with a larger number of models to understand the reasons for this model sensitivity. It should also be noted that our results are limited to partial assimilation experiments using only two climate models with anomaly/full field assimilations. Nevertheless, this study provides a blueprint for a multi-model approach using additional climate models and various experimental designs (e.g., full vs anomaly assimilation, pacemaker experiments, or flux-adjustment method) in order to identify the robust processes responsible and quantify the effects of model sensitivity.

5 Conclusion

Using an Atlantic Ocean partial assimilation approach, we evaluated the ENSO response to Atlantic forcing on interannual timescales. Our results imply a two-step process on how Atlantic Ocean variability affects ENSO evolution. First, tropical Atlantic SST warming induces a tropical SLP response with an atmospheric zonal wave-number 1 pattern through the reorganization of the Walker circulation, particularly at the equator. This tropical SLP response is accompanied by the strengthened surface trade winds over the western Pacific, which, in turn, affect the probability of a La Niña development by activating the Bjerknes feedback in the tropical Pacific. Since this process takes 7 months from the peak of Atlantic SST forcing to an SST response in the equatorial Pacific, it is possible that ENSO predictability can be extended for a few seasons by utilizing the Atlantic precursor signal as demonstrated by statistical and dynamical predictions (Frauen & Dommenget, 2012; Keenlyside et al., 2013; Dayan et al., 2014; Martín-Rey et al., 2015). Many previous studies have focused on the seasonal relationship how the summer Atlantic Niño affects the following winter Pacific La Niña particularly after 1970 (Rodríguez-Fonseca et al., 2009; Ding et al., 2012; Martín-Rey et al., 2015). Our analysis moves one step further by demonstrating that the equatorial Atlantic impact on the tropical Pacific can be found in any season although the summer Atlantic Niño still elicits the largest contributions to ENSO.

Among our multi-model experiments, there is a different response time between the western Pacific trade wind and the remote forcing from the Atlantic. After the equatorial Atlantic SST anomalies have peaked, we find eastward propagation of SLP anomalies from the Atlantic to the western Pacific via the Indian Ocean (Fig. 4b). The propagation speed over the Indian Ocean is slowest in the MIROC ATL anomaly run and fastest in the CESM ATL anomaly run (Fig. 4c–e). These propagation speeds indicate a model dependency as evident in the different timing for local peaks of correlation coefficients between Atlantic SST anomalies and anomalous zonal winds (Fig. 6a). Consistent with these SLP responses, the MIROC ATL run demonstrates the significant Walker circulation changes over the Indian Ocean and the subsequent SST response, whereas these features are unclear in CESM ATL anomaly and full runs. The impact of Atlantic mean state bias on ENSO potential predictability has an important implication under global warming, since the Atlantic-Pacific connection may weaken in a warmer climate (Jia et al., 2019).

Acknowledgments

The CESM experiment in this paper was conducted by the University of Southern California Center for High-Performance Computing and Communications (`http://hpcc.usc.edu`) and the high-performance computing support from Yellowstone (ark:/85065/d7wd3xhc) and Cheyenne (doi:10.5065/D6RX99HX) provided by NCAR's Computational and Information Systems Laboratory sponsored by the National Science Foundation. The MIROC experiment was supported by the Japanese Ministry of Education, Culture, Sports, Science and Technology, through the Program for Risk Information on Climate Change. The simulations were performed with the Earth Simulator at the Japan Agency for Marine Earth Science and Technology. ERSSTv4 and NCEP data sets are provided by the NOAA/OAR/ESRL PSD, Boulder, Colorado, USA, from their web site at `http://www.esrl.noaa.gov/psd/`. JRA55 and ProjD were provided by Japan Meteorological Agency through their web site at `https://jra.kishou.go.jp/JRA-55/index_en.html` and `https://climate.mri-jma.go.jp/pub/ocean/ts/`. The data in partial assimilation experiments are available from Utah Climate Center Web site at `https://climate.usu.edu/people/yoshi/data/2020-ENSO_Atl/data.html`. The manuscript benefited from the constructive comments of three anonymous reviewers. YC and SYW are supported by the Utah Agricultural Experiment Station, Utah State University, (approved as journal paper number 9230), SERDP Award RC19-F1-1389, and the U.S. Department of Interior, Bureau of Reclamation (R18AC00018, R19AP00149). SYW is also supported by U.S. Department of Energy under Award Number DE-SC0016605. MJM is supported by NOAA (PMEL contribution no. 4970). TM is supported by JSPS KAKENHI Grant Numbers JP19H05703 and JP17K05661.

References

Balmaseda, M. A., Mogensen, K., & Weaver, A. T. (2013). Evaluation of the ECMWF ocean reanalysis system ORAS4. *Quarterly Journal of the Royal Meteorological Society*, *139*(674), 1132–1161.

Barichivich, J., Gloor, E., Peylin, P., Brienen, R. J., Schöngart, J., Espinoza, J. C., & Pattnayak, K. C. (2018). Recent intensification of Amazon flooding extremes driven by strengthened walker circulation. *Science advances*, *4*(9), eaat8785.

Bloom, S. C., Takacs, L., da Silva, A. M., & Ledvina, D. (1996). Data assimilation using incremental analysis updates. *Mon. Wea. Rev.*, *124*, 1256-1271.

Boer, G. J., Smith, D. M., Cassou, C., Doblas-Reyes, F., Danabasoglu, G., Kirtman, B., ... others (2016). The decadal climate prediction project (DCPP) contribution to CMIP6. *Geoscientific Model Development (Online)*, *9*(10).

Cai, W., Wu, L., Lengaigne, M., Li, T., McGregor, S., Kug, J.-S., ... Chang, P. (2019). Pantropical climate interactions. *Science*, *363*(6430). Retrieved from http://science.sciencemag.org/content/363/6430/eaav4236 doi: 10.1126/science.aav4236

Capotondi, A., Wittenberg, A. T., Newman, M., Di Lorenzo, E., Yu, J.-Y., Braconnot, P., ... others (2015). Understanding ENSO diversity. *Bulletin of the American Meteorological Society*, *96*(6), 921–938.

Chikamoto, Y., Kimoto, M., Ishii, M., Mochizuki, T., Sakamoto, T. T., Tatebe, H., ... others (2013). An overview of decadal climate predictability in a multi-model ensemble by climate model MIROC. *Climate Dynamics*, *40*, 1201–1222.

Chikamoto, Y., Kimoto, M., Ishii, M., Watanabe, M., Nozawa, T., Mochizuki, T., ... Jin, F. (2012). Predictability of a stepwise shift in Pacific climate during the late 1990s in hindcast experiments using MIROC. *J. Meteorol. Soc. Japan*, *90A*, 1–21.

Chikamoto, Y., Mochizuki, T., Timmermann, A., Kimoto, M., & Watanabe, M. (2016). Potential tropical Atlantic impacts on Pacific decadal climate trends. *Geophysical Research Letters*, *43*(13), 7143–7151.

Chikamoto, Y., Timmermann, A., Luo, J.-J., Mochizuki, T., Kimoto, M., Watanabe, M., ... Jin, F.-F. (2015). Skillful multi-year predictions of tropical trans-basin climate variability. *Nature Communications*, *6*, 6869.

Chikamoto, Y., Timmermann, A., Widlansky, M. J., Balmaseda, M. A., & Stott, L. (2017). Multi-year predictability of climate, drought, and wildfire in southwestern North America. *Scientific Reports*, *7*(1), 6568.

Chikamoto, Y., Timmermann, A., Widlansky, M. J., Zhang, S., & Balmaseda, M. A. (2019). A drift-free decadal climate prediction system for the community earth syetem model. *Journal of Climate*, *published online*. doi: doi.org/10.1175/JCLI-D-18-0788.1

Dayan, H., Vialard, J., Izumo, T., & Lengaigne, M. (2014). Does sea surface temperature outside the tropical Pacific contribute to enhanced ENSO predictability?

Climate dynamics, *43*(5-6), 1311–1325.

Ding, H., Greatbatch, R. J., Latif, M., & Park, W. (2015). The impact of sea surface temperature bias on equatorial Atlantic interannual variability in partially coupled model experiments. *Geophysical Research Letters*, *42*(13), 5540–5546.

Ding, H., Keenlyside, N., Latif, M., Park, W., & Wahl, S. (2015). The impact of mean state errors on equatorial Atlantic interannual variability in a climate model. *Journal of Geophysical Research: Oceans*, *120*(2), 1133–1151.

Ding, H., Keenlyside, N. S., & Latif, M. (2012). Impact of the equatorial Atlantic on the El Niño southern oscillation. *Climate dynamics*, *38*(9-10), 1965–1972.

Dippe, T., Greatbatch, R. J., & Ding, H. (2019). Seasonal prediction of equatorial Atlantic sea surface temperature using simple initialization and bias correction techniques. *Atmospheric Science Letters*, *20*(5), e898.

Dong, L., & McPhaden, M. J. (2018). Unusually warm Indian Ocean sea surface temperatures help to arrest development of El Niño in 2014. *Scientific reports*, *8*(1), 2249.

Enfield, D. B., & Mayer, D. A. (1997). Tropical Atlantic sea surface temperature variability and its relation to El Niño-Southern Oscillation. *J. Geophys. Res.*, *102*, 929-945.

Fosu, B., He, J., & Wang, S.-Y. S. (2020). The influence of wintertime SST variability in the Western North Pacific on ENSO diversity. *Climate Dynamics*, 1–14.

Frauen, C., & Dommenget, D. (2012). Influences of the tropical Indian and Atlantic Oceans on the predictability of ENSO. *Geophysical Research Letters*, *39*(2).

Ham, Y.-G., Kug, J.-S., & Park, J.-Y. (2013). Two distinct roles of Atlantic SSTs in ENSO variability: North tropical Atlantic SST and Atlantic Niño. *Geophysical Research Letters*, *40*(15), 4012–4017.

Ham, Y.-G., Kug, J.-S., Park, J.-Y., & Jin, F.-F. (2013). Sea surface temperature in the north tropical Atlantic as a trigger for El Niño/Southern Oscillation events. *Nature Geoscience*, *6*(2), 112.

Handoh, I. C., Matthews, A. J., Bigg, G. R., & Stevens, D. P. (2006). Interannual variability of the tropical Atlantic independent of and associated with ENSO: Part I. The North Tropical Atlantic. *International journal of climatology*, *26*(14), 1937–1956.

Huang, B., Banzon, V. F., Freeman, E., Lawrimore, J., Liu, W., Peterson, T. C., …

Zhang, H.-M. (2015). Extended reconstructed sea surface temperature version 4 (ERSST. v4). Part I: upgrades and intercomparisons. *Journal of Climate*, *28*(3), 911–930.

Huang, B., Kinter, J., & Schopf, P. (2002). Ocean data assimilation using intermittent analyses and continuous model error correction. *Adv. Atmos. Sci.*, *19*(6), 965–992.

Ishii, M., & Kimoto, M. (2009). Reevaluation of historical ocean heat content variations with time-varying XBT and MBT depth bias corrections. *J. Oceanogr.*, *65*(3), 287–299.

Izumo, T., Lengaigne, M., Vialard, J., Luo, J.-J., Yamagata, T., & Madec, G. (2014). Influence of Indian Ocean Dipole and Pacific recharge on following year's El Niño: interdecadal robustness. *Climate dynamics*, *42*(1-2), 291–310.

Izumo, T., Vialard, J., Lengaigne, M., de Boyer Montegut, C., Behera, S. K., Luo, J.-J., ... Yamagata, T. (2010). Influence of the state of the Indian Ocean Dipole on the following year's El Niño. *Nature Geoscience*, *3*(3), 168.

Jia, F., Cai, W., Wu, L., Gan, B., Wang, G., Kucharski, F., ... Keenlyside, N. (2019). Weakening Atlantic Niño–Pacific connection under greenhouse warming. *Science advances*, *5*(8). doi: 10.1126/sciadv.eaax4111

Jin, F.-F. (1997). An equatorial ocean recharge paradigm for ENSO. Part I: conceptual model. *J. Atmos. Sci.*, *54*, 811-829.

Johnson, Z. F., Chikamoto, Y., Wang, S.-Y. S., McPhaden, M. J., & Mochizuki, T. (2020). Pacific decadal oscillation remotely forced by the equatorial pacific and the atlantic oceans. *Climate Dynamics*. doi: doi.org/10.1007/s00382-020-05295-2

Kajtar, J. B., Santoso, A., McGregor, S., England, M. H., & Baillie, Z. (2018). Model under-representation of decadal Pacific trade wind trends and its link to tropical Atlantic bias. *Climate Dynamics*, *50*(3-4), 1471–1484.

Kalnay, E., Kanamitsu, M., Kistler, R., Deaven, W. C. D., Gandin, L., Iredell, M., ... Joseph, D. (1996). The NCEP/NCAR 40-year reanalysis project. *Bull. Amer. Meteorol. Soc.*, *77*, 437-471.

Keenlyside, N. S., Ding, H., & Latif, M. (2013). Potential of equatorial Atlantic variability to enhance El Niño prediction. *Geophysical Research Letters*, *40*(10), 2278–2283.

Kobayashi, S., Ota, Y., Harada, Y., Ebita, A., Moriya, M., Onoda, H., ... others (2015). The JRA-55 reanalysis: General specifications and basic characteristics. *Journal of the Meteorological Society of Japan. Ser. II*, *93*(1), 5–48.

Kosaka, Y., & Xie, S.-P. (2013). Recent global-warming hiatus tied to equatorial Pacific surface cooling. *Nature*, *501*(7467), 403–407.

Kucharski, F., Ikram, F., Molteni, F., Farneti, R., Kang, I.-S., No, H.-H., ... Mogensen, K. (2016). Atlantic forcing of Pacific decadal variability. *Climate Dynamics*, *46*(7-8), 2337–2351.

Kucharski, F., Kang, I., Farneti, R., & Feudale, L. (2011). Tropical Pacific response to 20th century Atlantic warming. *Geophys. Res. Lett.*, *38*, L03702.

Latif, M., & Grötzner, A. (2000). The equatorial Atlantic oscillation and its response to ENSO. *Climate Dynamics*, *16*(2-3), 213–218.

Levine, A. F., Frierson, D. M., & McPhaden, M. J. (2018). AMO forcing of multidecadal Pacific ITCZ variability. *Journal of Climate*, *31*(14), 5749–5764.

Levine, A. F., McPhaden, M. J., & Frierson, D. M. (2017). The impact of the AMO on multidecadal ENSO variability. *Geophysical Research Letters*, *44*(8), 3877–3886.

Li, X., Xie, S.-P., Gille, S. T., & Yoo, C. (2015). Atlantic-induced pan-tropical climate change over the past three decades. *Nature Climate Change*. doi: 10.1038/nclimate2840

Lübbecke, J. F., & McPhaden, M. J. (2012). On the inconsistent relationship between Pacific and Atlantic Niños. *Journal of Climate*, *25*(12), 4294–4303.

Luo, J.-J., Wang, G., & Dommenget, D. (2018). May common model biases reduce CMIP5's ability to simulate the recent Pacific La Niña-like cooling? *Climate Dynamics*, *50*(3-4), 1335–1351.

Martín-Rey, M., Rodríguez-Fonseca, B., & Polo, I. (2015). Atlantic opportunities for ENSO prediction. *Geophysical Research Letters*, *42*(16), 6802–6810.

Martín-Rey, M., Rodríguez-Fonseca, B., Polo, I., & Kucharski, F. (2014). On the Atlantic–Pacific Niños connection: a multidecadal modulated mode. *Climate dynamics*, *43*(11), 3163–3178.

McGregor, S., Stuecker, M. F., Kajtar, J. B., England, M. H., & Collins, M. (2018). Model tropical Atlantic biases underpin diminished Pacific decadal variability. *Nature Climate Change*, *8*, 493–498.

McGregor, S., Timmermann, A., Stuecker, M. F., England, M. H., Merrifield, M., Jin, F.-F., & Chikamoto, Y. (2014). Recent Walker circulation strengthening and Pacific cooling amplified by Atlantic warming. *Nature Climate Change*, *4*(10), 888–892.

McPhaden, M. J. (2003). Tropical Pacific Ocean heat content variations and ENSO persistence barriers. *Geophysical research letters*, *30*(9).

Meinen, C. S., & McPhaden, M. J. (2000). Observations of warm water volume changes in the equatorial Pacific and their relationship to El Niño and La Niña. *Journal of Climate*, *13*(20), 3551–3559.

Mochizuki, T., Chikamoto, Y., Kimoto, M., Ishii, M., Tatebe, H., Komuro, Y., ... Mori, M. (2012). Decadal prediction using a recent series of MIROC global climate models. *J. Meteorol. Soc. Japan*, *90A*, 373–383. (submitted) doi: 10.2151/jmsj.2012-A22

Mochizuki, T., Ishii, M., Kimoto, M., Chikamoto, Y., Watanabe, M., Nozawa, T., ... Mori, M. (2010). Pacific decadal oscillation hindcasts relevant to near-term climate prediction. *Proc. Natl. Acad. Sci. USA*, *107*, 1833. (doi:10.1073/pnas.0906531107)

Nozawa, T., Nagashima, T., Ogura, T., Yokohata, T., Okada, N., & Shiogama, H. (2007). Climate change simulations with a coupled ocean-atmosphere GCM called the model for interdisciplinary research on climate: MIROC. *CGER Supercomput. Monogr. Rep*, *12*. (Cent. for Global Environ. Res., Natl. Inst. for Environ. Stud., Tsukuba, Japan.)

Polo, I., Martin-Rey, M., Rodriguez-Fonseca, B., Kucharski, F., & Mechoso, C. R. (2015). Processes in the Pacific La Niña onset triggered by the Atlantic Niño. *Climate dynamics*, *44*(1-2), 115–131.

Richter, I. (2015). Climate model biases in the eastern tropical oceans: Causes, impacts and ways forward. *Wiley Interdisciplinary Reviews: Climate Change*, *6*(3), 345–358.

Rodríguez-Fonseca, B., Polo, I., García-Serrano, J., Losada, T., Mohino, E., Mechoso, C. R., & Kucharski, F. (2009). Are Atlantic Niños enhancing Pacific ENSO events in recent decades? *Geophysical Research Letters*, *36*(20).

Ruprich-Robert, Y., Msadek, R., Castruccio, F., Yeager, S., Delworth, T., & Danabasoglu, G. (2017). Assessing the climate impacts of the observed Atlantic multidecadal variability using the GFDL CM2.1 and NCAR CESM1 global coupled models. *Journal of Climate*, *30*(8), 2785–2810.

Sasaki, W., Doi, T., Richards, K. J., & Masumoto, Y. (2014). Impact of the equatorial Atlantic sea surface temperature on the tropical Pacific in a CGCM. *Climate dynamics*, *43*(9-10), 2539–2552.

Shields, C. A., Bailey, D. A., Danabasoglu, G., Jochum, M., Kiehl, J. T., Levis, S., & Park, S. (2012). The low-resolution CCSM4. *Journal of Climate*, *25*(12), 3993–4014.

Tatebe, H., Ishii, M., Mochizuki, T., Chikamoto, Y., Sakamoto, T. T., Komuro, Y., ... Kimoto, M. (2012). The initialization of the MIROC climate models with hydrographic data assimilation for decadal prediction. *J. Meteorol. Soc. Japan*, *90A*, 275–294. doi: 10.2151/jmsj.2012-A14

Timmermann, A., An, S.-I., Kug, J.-S., Jin, F.-F., Cai, W., Capotondi, A., ... others (2018). El Niño–Southern Oscillation complexity. *Nature*, *559*(7715), 535.

Tokinaga, H., Richter, I., & Kosaka, Y. (2019). ENSO influence on the Atlantic Niño, revisited: Multi-year versus single-year ENSO events. *Journal of Climate*, *32*(14), 4585-4600. doi: 10.1175/JCLI-D-18-0683.1

Wang, C., & Picaut, J. (2004). Understanding ENSO physics—a review. *Earth Climate: Ocean-atmosphere interaction and climate variability*, *147*, 21-48. (Geophysical Monograph, AGU, Washington D. C.)

Wang, L., Yu, J.-Y., & Paek, H. (2017). Enhanced biennial variability in the Pacific due to Atlantic capacitor effect. *Nature communications*, *8*, 14887.

Wang, S.-Y., L'Heureux, M., & Yoon, J.-H. (2013). Are greenhouse gases changing ENSO precursors in the western North Pacific? *Journal of Climate*, *26*(17), 6309–6322.

Wang, S.-Y. S., Jiang, X., & Fosu, B. (2015). Global eastward propagation signals associated with the 4–5-year ENSO cycle. *Climate Dynamics*, *44*(9-10), 2825–2837.

Xie, S., Hu, K., Hafner, J., Tokinaga, H., Du, Y., Huang, G., & Sampe, T. (2009). Indian Ocean capacitor effect on Indo-western Pacific climate during the summer following El Niño. *J. Climate*, *22*(3), 730–747.

Xie, S. P., & Carton, J. A. (2004). Tropical Atlantic variability: patterns, mechanisms, and impacts. *Earth Climate: ocean-atmosphere interaction and climate variability*, *147*, 121-142. (Geophysical Monograph, AGU, Washington D. C.)

Table 1. Summary of (a) decadal climate prediction experiments and (b) Atlantic ocean data assimilation experiments. The 5-year and 2-year model spin-up periods for the Atlantic partial assimilation experiments are excluded in MIROC and CESM runs, respectively.

(a) Decadal climate prediction experiment

Experiment	Brief description
Historical runs	Prescribing natural and anthropogenic radiative forcing to climate models.
Assimilation runs	Assimilating the observed ocean anomalies while prescribing the forcing.
Hindcast runs	10-year-long hindcast experiments initialized on January 1^{st} every year.

(b) Atlantic partial ocean data assimilation experiments

Name	Model	Region	Ocean field	Ensemble	Period
MIROC ATL anomaly	MIROC3.2	Atlantic	Anomaly	10-member	1950–2009
CESM ATL anomaly	CESM1.0	Atlantic	Anomaly	10-member	1960–2014
CESM ATL full	CESM1.0	Atlantic	Full	10-member	1960–2014

Table 2. Potential predictability of Niño 3.4, Niño 4, and Indo-Pacific zonal wind indices (zonal wind anomalies at 850 hPa averaged in 5°S–5°N, 90°E–150°E) measured by an anomaly correlation coefficient between observation and ATL run.

Run	Niño 4	Niño 3.4	Niño 3	zonal wind
MIROC ATL anomaly	0.31	0.24	0.14	0.23
CESM ATL anomaly	0.04	0.06	0.02	0.18
CESM ATL full	0.25	0.22	0.14	0.46
Multi-model	0.27	0.22	0.13	0.36

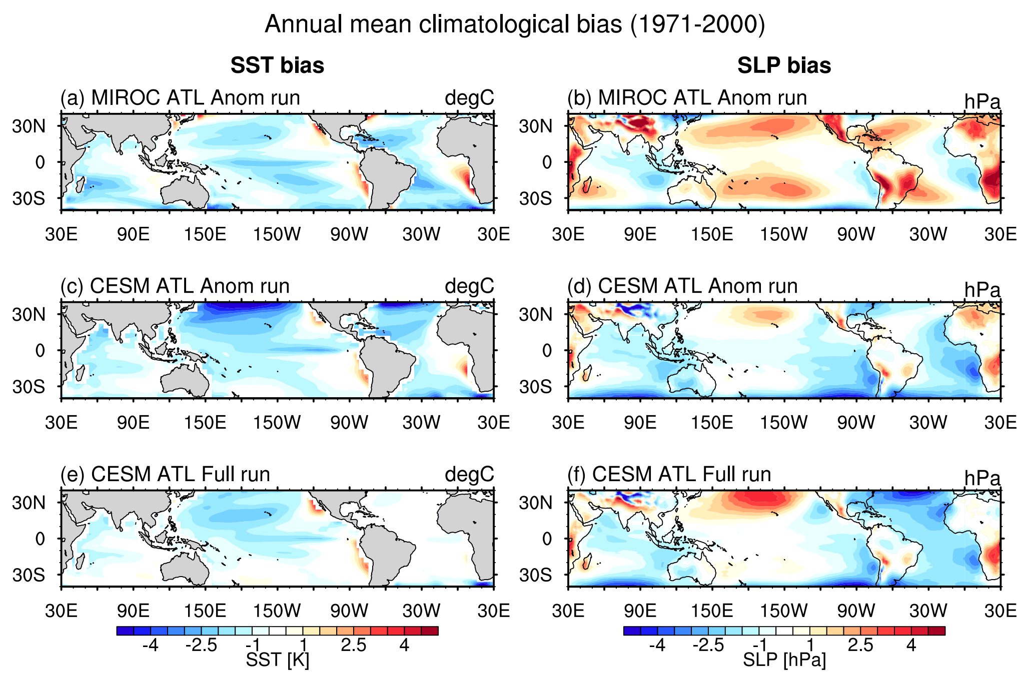

Figure 1. Annual mean climatological biases of SST (left) and SLP (right panels) for (a, b) MIROC ATL anomaly run, (c, d) CESM ATL anomaly run, and (e ,f) CESM ATL full run, compared to observations. Annual mean climatology is obtained for a reference period 1971–2000.

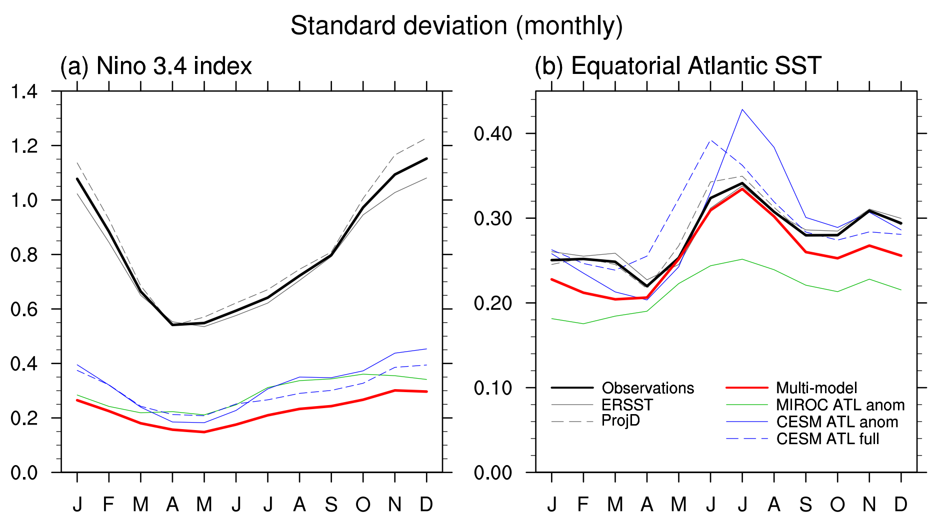

Figure 2. Standard deviations of the monthly (a) Niño3.4 index and (b) SST anomalies averaged over the equatorial Atlantic in observations (black) and the ATL runs (color lines).

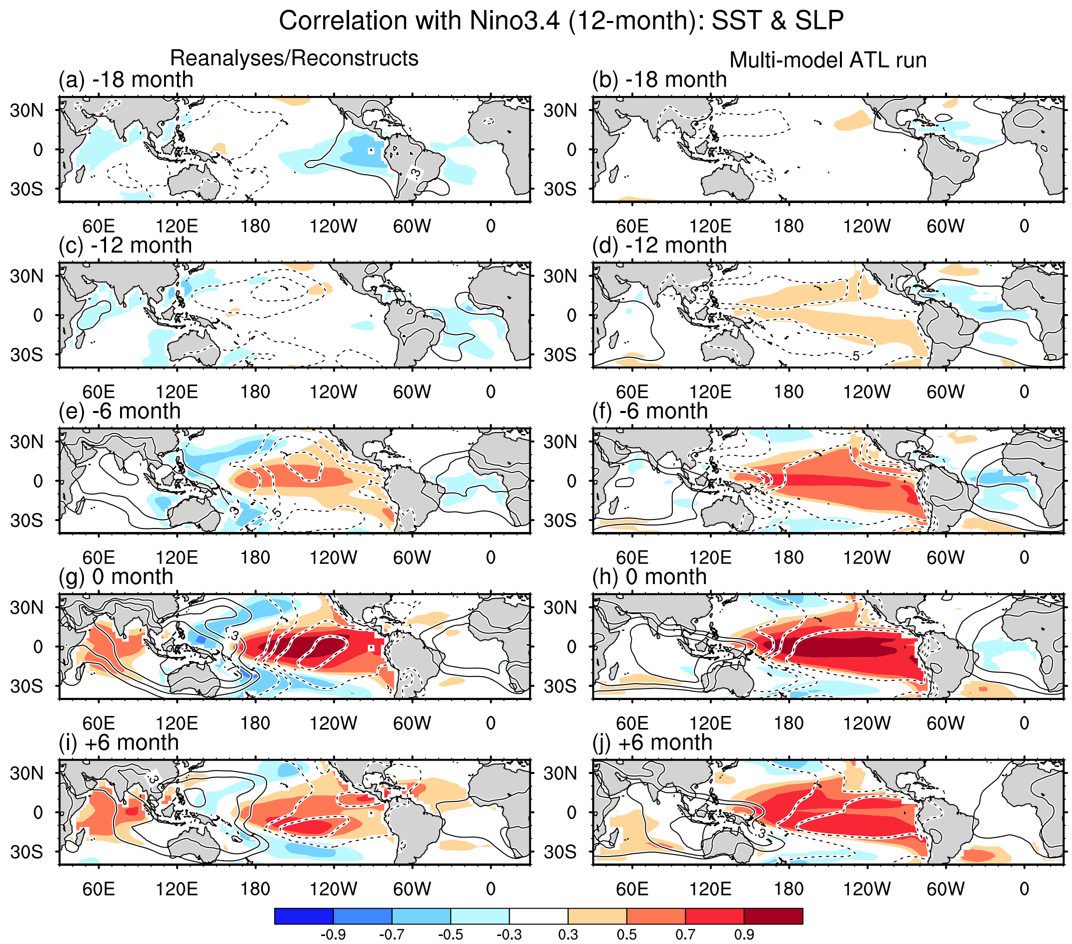

Figure 3. Correlation maps of SST (shaded) and SLP anomalies (contoured) with the Niño 3.4 index in observations (left) and multi-model ensemble of the ATL runs (right panels) at (a,b) −18, (c,d) −12, (e,f) −6, (g,h) 0, and (i,j) +6 month lags. The contour interval is ±0.3, ±0.5, ±0.7, and ±0.9. Negative contours are dashed and the zero contour is omitted. A 12-month running mean filter is applied to anomalies after detrending. A correlation coefficient of 0.29 corresponds to the statistical significant at 95% levels with 48 degrees of freedom on the basis of two-side Student's t-test.

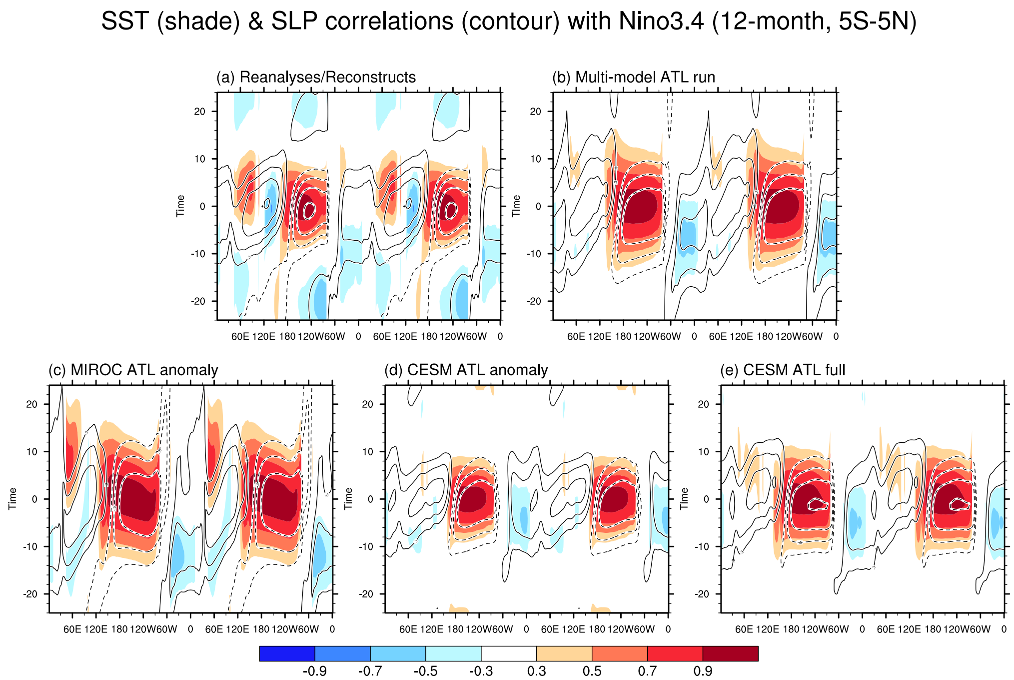

Figure 4. Lead-lag correlations of SLP (contours) and SST anomalies (shaded) correlated with the Niño 3.4 index at the equator (5°S–5°N) in (a) observations, (b) multi-model ATL run, and its individual experiment for (c) MIROC ATL anomaly, (d) CESM ATL anomaly, and (e) CESM ATL full runs. Note that longitude is repeated twice. Positive (negative) lags indicate that the Niño 3.4 index is leading (lagging) the anomalies. Negative contours are dashed and the zero contour is omitted. The contour interval is ±0.3, ±0.5, ±0.7, and ±0.9. A correlation coefficient of 0.29 corresponds to the statistical significant at 95% levels with 48 degrees of freedom on the basis of two-side Student's t-test.

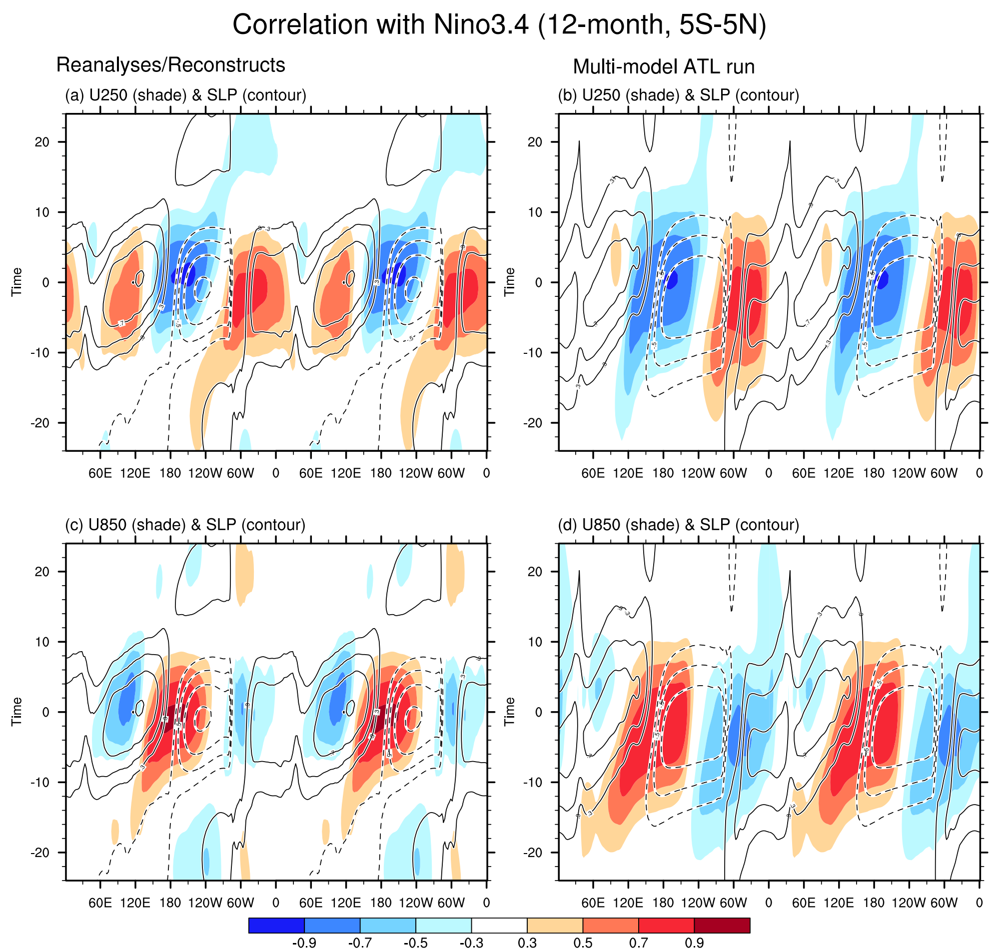

Figure 5. Lead-lag correlations of SLP (contours), (a,b) zonal wind anomalies at 250 hPa (shading) and (c,d) 850 hPa (shading) correlated with the Niño 3.4 index at the equator (5°S–5°N) in observations (left) and multi-model mean of ATL runs (right panels). Note that longitude is repeated twice. Positive (negative) lags indicate that the Niño 3.4 index is leading (lagging) the anomalies. Negative contours are dashed and the zero contour is omitted. The contour interval is ±0.3, ±0.5, ±0.7, and ±0.9. A correlation coefficient of 0.29 corresponds to the statistical significant at 95% levels with 48 degrees of freedom on the basis of two-side Student's t-test.

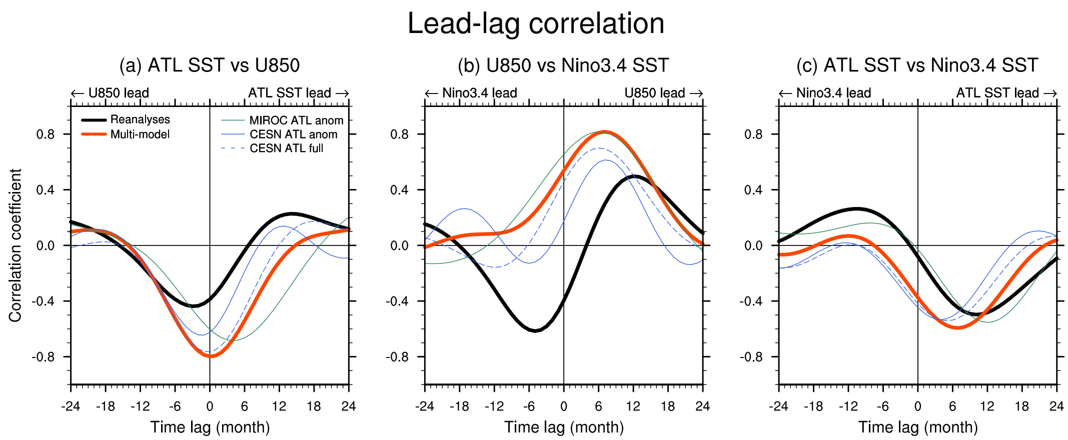

Figure 6. Lead-lag correlations between (a) equatorial Atlantic SST (5°S–5°N, 50°W–0°) and zonal wind anomalies at 850 hPa in the Indo-Pacific region (5°S–5°N, 90°E–150°E), (b) zonal wind anomalies at 850 hPa in the Indo-Pacific region and Nino 3.4 index (SST anomalies in 5°S–5°N, 170°W–120°W), and (c) equatorial Atlantic SST and Nino 3.4 index. Black and red lines are observations and multi-model ensemble of ATL runs, respectively. Green, blue solid and blue dashed lines correspond to the MIROC ATL anomaly, CESM ATL anomaly, and CESM ATL full runs, respectively.

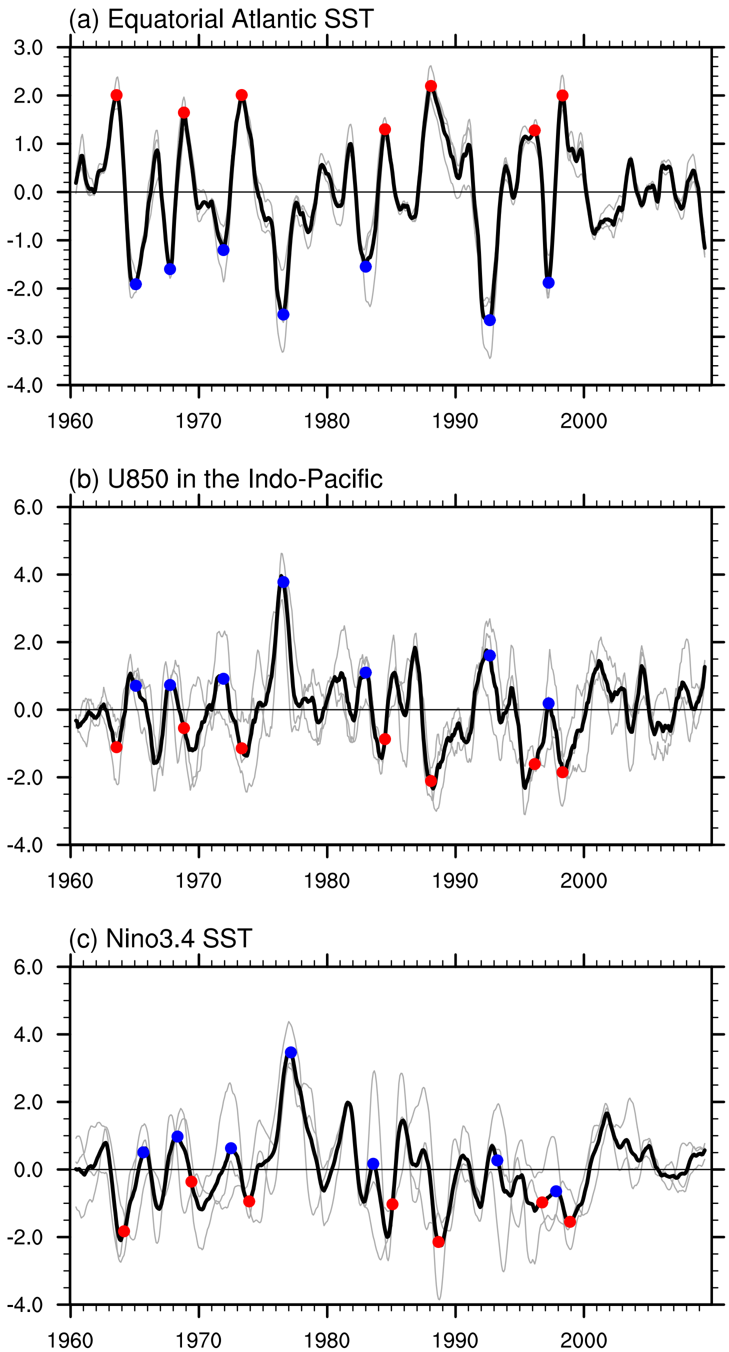

Figure 7. Standardized timeseries of (a) the equatorial Atlantic SST anomalies, (b) anomalous zonal wind at 850 hPa in the Indo-Pacific region, and (c) Niño 3.4 index in the ATL runs. Thick and thin lines are the multi-model ensemble mean of ATL runs and the 10-member ensemble mean of individual ATL run (i.e., CESM ATL anomaly, CESM ATL full and MIROC ATL anomaly runs), respectively. Red and blue circles correspond to the warmer and colder months of equatorial Atlantic SST anomalies in (a, b) but for +7 month lag in (c).

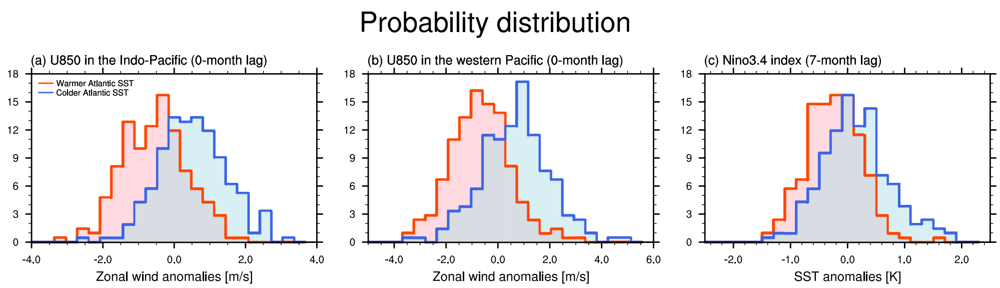

Figure 8. Histograms of (a) zonal wind anomalies at 850 hPa in the Indo-Pacific region (5°S–5°N, 90°E–150°E) at 0-month lag, (b) zonal wind anomalies at 850 hPa in the western Pacific region (5°S–5°N, 120°E–150°E) at 0-month lag, and (c) SST anomalies in the Niño 3.4 region (5°S–5°N, 170°W–120°W) at 7-month lag associated with warmer (red) and colder (blue) tropical Atlantic SST anomalies (blue: 5°S–5°N, 50°W–0°) in each member of the ATL run. We extract 7 months of SST anomalies warmer than 1.5 standard deviation: Aug 1963, Nov 1968, May 1973, Jul 1984, Feb 1988, Mar 1996, May 1998; and 7 month colder than 1.5 standard deviation: Feb 1965, Oct 1967, Dec 1971, Aug 1976, Jan 1983, Sep 1992, Apr 1997 (see Fig. 7). There are 210 samples in these distributions (= 7 years $\times$ 10 members $\times$ 3 runs).

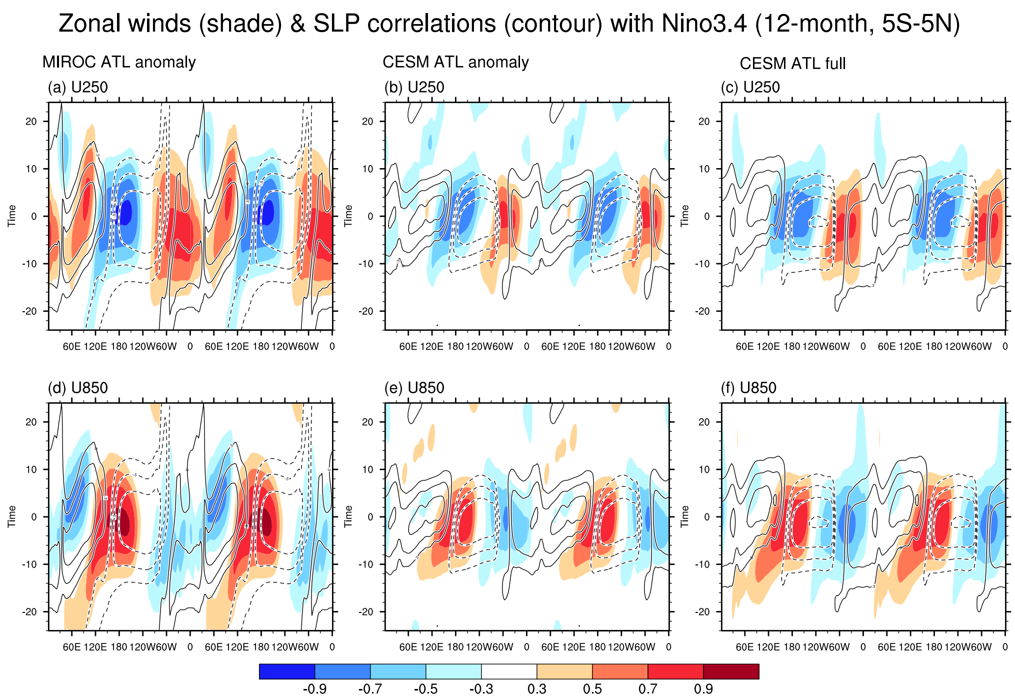

Figure 9. Lead-lag correlations of SLP (contours), zonal wind anomalies at 250 hPa (top) and 850 hPa (bottom) correlated with the Niño 3.4 index at the equator (5°S–5°N) in MIROC ATL anomaly (left), CESM ATL anomaly (center), and CESM ATL full runs (right panels). Note that longitude is repeated twice. Positive (negative) lags indicate that the Niño 3.4 index is leading (lagging) the anomalies. Negative contours are dashed and the zero contour is omitted. The contour interval is ±0.3, ±0.5, ±0.7, and ±0.9. A correlation coefficient of 0.29 corresponds to the statistical significant at 95% levels with 48 degrees of freedom on the basis of two-side Student's t-test.

Supporting Information for "El Niño Southern Oscillation evolution modulated by the Atlantic forcing"

Y. Chikamoto[1 *], Z. F. Johnson[1], S.-Y. Wang[1], M. J. McPhaden[2] and T. Mochizuki[3,4]

[1]Department of Plants, Soils & Climate, Utah State University, Logan, UT, USA

[2]Pacific Marine Environmental Laboratory/NOAA, Seattle, WA, USA

[3]Department of Earth and Planetary Sciences, Kyushu University, Fukuoka, Japan

[4]Japan Agency for Marine-Earth Science and Technology, Yokohama, Japan

Contents of this file

1. Figures S1 to S3

[*]4820 Old Main Hill, Logan, UT 84322-4820, USA

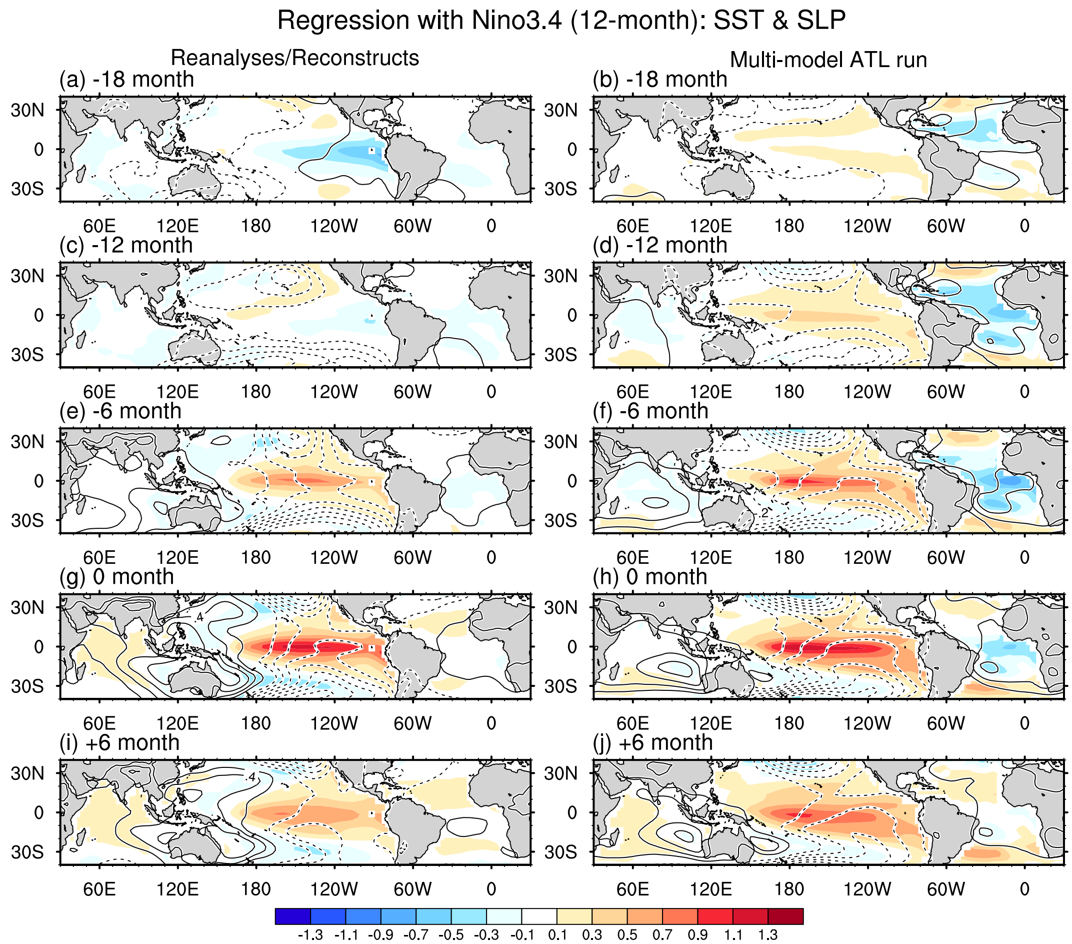

Figure S1. Regression maps of SST (shaded) and SLP anomalies (contoured) with the Niño 3.4 index in observations (left) and multi-model ensemble of the ATL runs (right panels) at (a,b) -18, (c,d) -12, (e,f) -6, (g,h) 0, and (i,j) $+6$ month lags. The contour interval is ± 0.2, ± 0.4, ± 0.6, ± 0.8, ± 1.0, ± 1.2, and ± 1.3 hPa. Negative contours are dashed and the zero contour is omitted. A 12-month running mean filter is applied to anomalies after detrending.

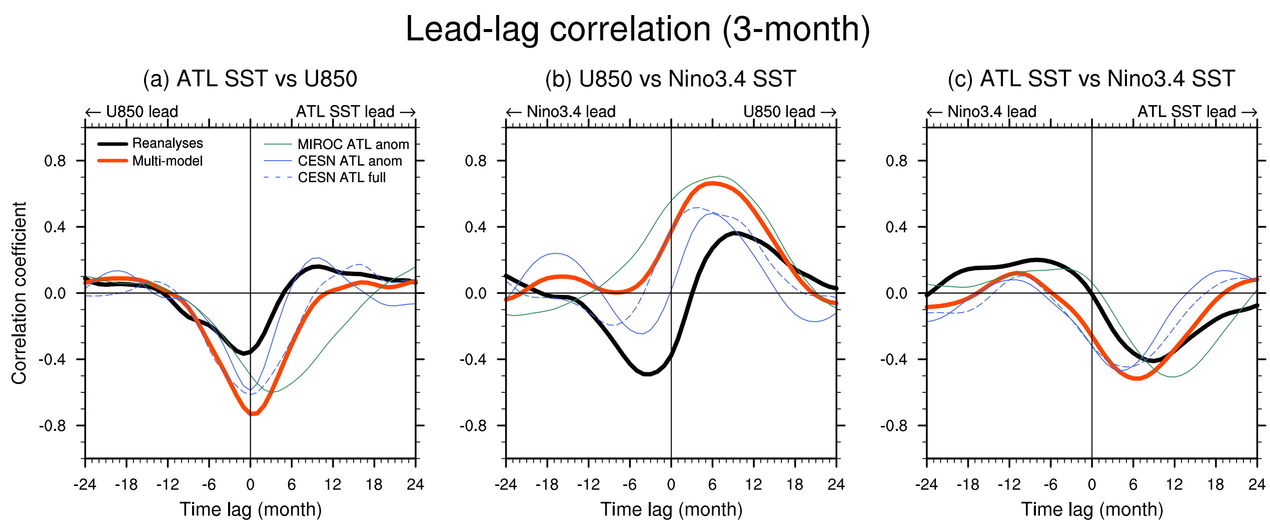

Figure S2. Lead-lag correlations between (a) equatorial Atlantic SST (5°S–5°N, 50°W–0°) and zonal wind anomalies at 850 hPa in the Indo-Pacific region (5°S–5°N, 90°E–150°E), (b) zonal wind anomalies at 850 hPa in the Indo-Pacific region and Nino 3.4 index (SST anomalies in 5°S–5°N, 170°W–120°W), and (c) equatorial Atlantic SST and Nino 3.4 index. Black and red lines are observations and multi-model ensemble of ATL runs, respectively. Green, blue solid and blue dashed lines correspond to the MIROC ATL anomaly, CESM ATL anomaly, and CESM ATL full runs, respectively. A 3-month running mean filter is applied to anomalies after detrending.

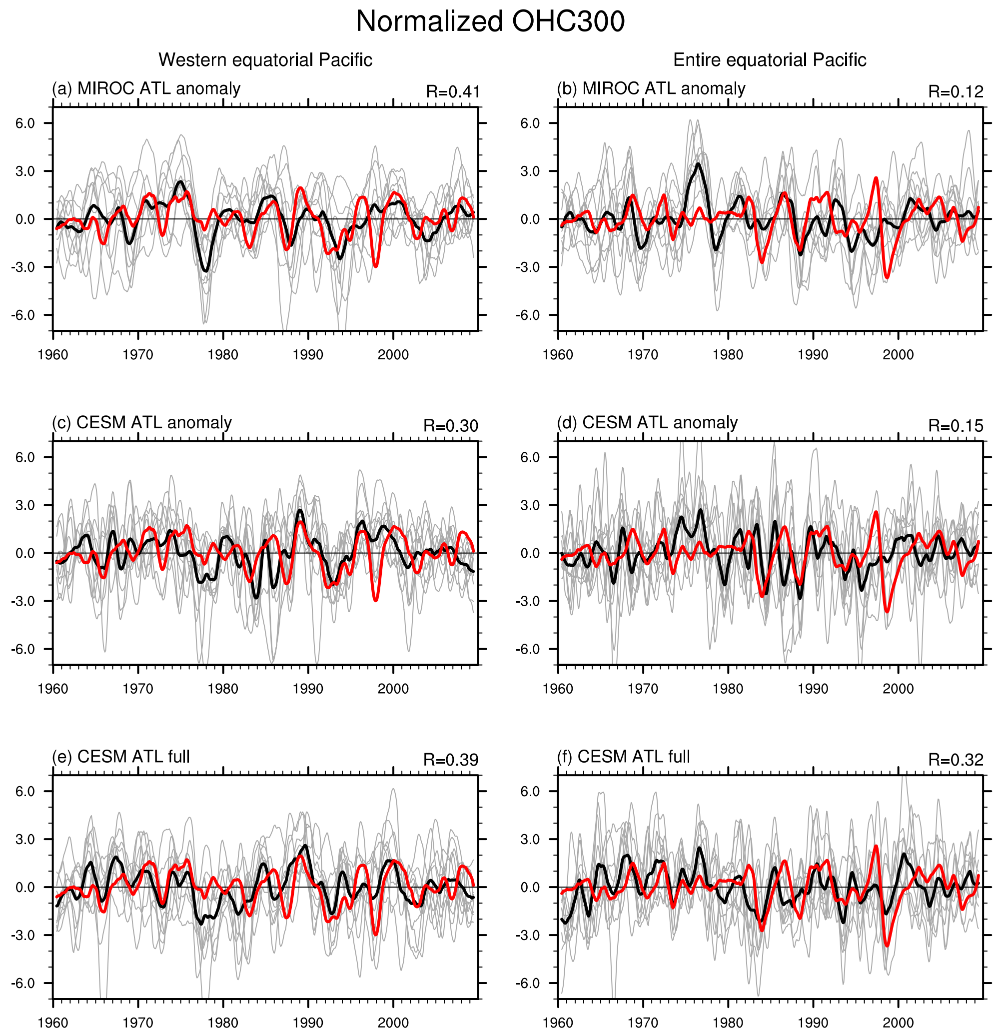

Figure S3. Timeseries of normalized upper ocean heat content at the western (left panels; 5°S–5°N, 120°E–165°E) and the entire equatorial Pacific (right panels; 5°S–5°N, 120°E–80°W) in (a, b) MIROC ATL anomaly, (c, d) CESM ATL anomaly, and (e, f) CESM ATL full runs. The upper ocean heat content is estimated by ocean heat content averaged from surface to 300 m depth. Red, black, and gray lines are the observations (ProjD), the ensemble mean, and each ensemble member, respectively. Anomalies are normalized by one standard deviations in the observation and the 10-ensemble mean. A correlation coefficient between the observation and the 10-ensemble mean is denoted at the upper-right corner.